

Journal für
Kardiologie

Austrian Journal of Cardiology

Österreichische Zeitschrift für Herz-Kreislaufkrankungen

**Evaluation of Congenital Heart
Disease and Cardiac Masses by
Magnetic Resonance Imaging**

Frank H

Journal für Kardiologie - Austrian

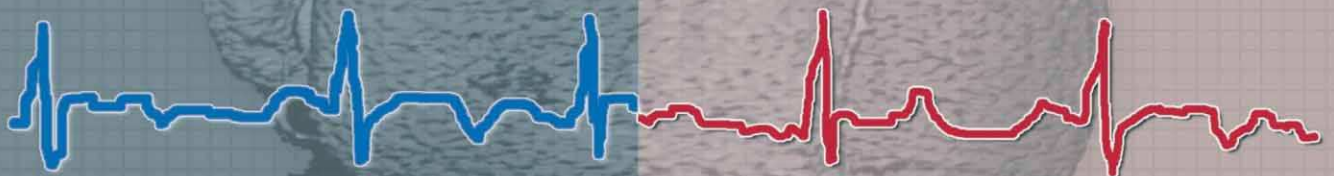
Journal of Cardiology 2003; 10

(1-2), 19-25

Homepage:

www.kup.at/kardiologie

**Online-Datenbank mit
Autoren- und Stichwortsuche**



Indexed in EMBASE/Excerpta Medica/SCOPUS

www.kup.at/kardiologie

Krause & Pachernegg GmbH · VERLAG für MEDIZIN und WIRTSCHAFT · A-3003 Gablitz

P.b.b. 02Z031105M, Verlagspostamt: 3002 Purkersdorf, Erscheinungsort: 3003 Gablitz

Evaluation of Congenital Heart Disease and Cardiac Masses by Magnetic Resonance Imaging

H. Frank

Abstract: As a tomographic method with a good spatial resolution, MRI allows identification of visceral atrial situs, type of ventricular loop, and relationship of the great vessels. From a comparison with angiographic and 2-D echocardiographic images, MRI provides accurate anatomic diagnosis in complex congenital heart diseases. In some instances, MRI can replace the need for invasive cardiac catheterization or reduce the number of catheterizations required in management of patients with complex congenital heart disease. MR imaging of complex congenital heart diseases is necessary for preoperative assessment in adults and in infants, and influences surgical planning by knowledge of the anatomic topography of the vascular malformation and relation to the bronchial system.

In cardiac tumors magnetic resonance imaging provides a non-invasive and three-dimensional assessment of masses involving the cardiac chambers, the pericardium, and the extracardiac structures. MRI has become an established method to yield complementary diagnostic information and to guide cardiac surgeons in the design of an appropriate therapeutic strategy. Furthermore, MRI allows to some extent characterization of tumor tissue. The

goal of MRI for assessing cardiac and paracardiac masses includes (1) to confirm or to exclude a mass suspected by X-ray or echocardiography, (2) to assess the location, mobility and its relationship to surrounding tissues, (3) to image the degree of vascularisation, (4) to distinguish solid from fluid lesions, and (5) to determine tissue characteristics and the specific nature of a mass.

Kurzfassung: Magnetresonanztomographie in der Diagnostik von kardialen Raumforderungen und komplexen kongenitalen Vitien. Die Magnetresonanztomographie (MR) wird vermehrt für die Diagnostik von komplexen kongenitalen Vitien, auch vorwiegend im pädiatrischen Bereich sowie in der Nachkontrolle, eingesetzt.

Durch den Vorteil des großen Field-of-view (FOV) können Gefäßanomalien sowie intrathorakale Malformationen sowohl auf normalen Spinecho-Sequenzen wie auch auf Gradientenecho-Sequenzen diagnostiziert werden. Aus diesem Grund sind kongenitale Vitien wie DAB, TOF, DORV, TGA etc. mittels MR gut beurteilbar. Auch im Follow-up, gerade durch die Beurteilung von Regurgitationsvolumina, durch die velocity encoded CINE-MR-

Technik bei Pulmonalinsuffizienz, ist diese nichtinvasive bildgebende Methode als geeignet anzusehen.

Bezüglich der intra- und extrakardialen Raumforderungen ist die MR gerade durch Verwendung von T2-Sequenzen und Gadolinium-DTPA eine für den klinischen Alltag wesentliche Technik. Durch den Vorteil einer Gewebedifferenzierung aufgrund der unterschiedlichen Signalintensitäten trägt die MR in der wesentlichen Tumordiagnostik bei. So weisen maligne Raumforderungen ein stärkeres Signal-Enhancement auf als benigne. Kriterien der Malignität sind weiters das Vorliegen eines hämorrhagischen Perikardergusses sowie das infiltrative Wachstum. Alle diese Kriterien können durch Beurteilung der morphologischen Verhältnisse mittels T1 und T2 sowie durch Kontrastmittelgabe beurteilt werden.

Zusammenfassend ist die MR sowohl in der Beurteilung von komplexen kongenitalen Vitien, aber auch in der Diagnostik von intra- und extrakardialen Tumoren ein wesentliches und bedeutendes Untersuchungsverfahren, das auch für die Planung chirurgischer Eingriffe wesentliche Zusatzinformationen bietet. **J Kardiologie 2003; 10: 19–25.**

■ Congenital Heart Disease

As a tomographic method with good spatial resolution, MRI allows the identification of visceral atrial situs, type of ventricular loop, and relationship of the great vessels [1]. From a comparison with angiographic and 2-D echocardiographic images, MRI provides accurate anatomic diagnosis in complex congenital heart diseases. In some instances, MRI can replace the need for invasive cardiac catheterization or reduce the number of catheterizations required in the management of patients with complex congenital heart disease. MR imaging of complex congenital heart diseases is necessary for pre-operative assessment in adults and in infants, and influences surgical planning by knowledge of the anatomic topography of the vascular malformation and relation to the bronchial system.

Atrial Septal Defect

Visualization of atrial septum defects (ASD) by MRI with SE-technique is well established, as is the use of dynamic imaging with GRE-technique to visualize ASD shunt flow [2]. SE-technique allows delineation of the atrial septum in two orthogonal views (short axis and four chamber) perpendicular to the plane of the septum. Large atrial septal defects can be easily identified as absence of, or a large deficit in, the interatrial septum. MRI has high sensitivity and specificity in the diagnosis of primum, secundum and sinus venosus ASDs [1]. False positive diagnoses of ASDs can occur due to the low signal intensity of the atrial septum in the region of the fossa

ovalis. The differentiation between signal dropout in the area of the fossa ovalis and a true secundum atrial defect is especially difficult in images of suboptimal quality. Thus, SE imaging can give erroneously large measurements of secundum ASD size. Ostium primum and sinus venosus ASDs are located primarily in thicker parts of the septum, these lesions being defined more reliably by septal discontinuity in SE images [3].

Dynamic imaging with GRE-technique can visualize ASD shunt jet, especially in increased interatrial pressure gradients. However, this technique may be inadequate, if the jet velocity is low, in presence of a low interatrial pressure gradient. In such cases, shunt flow can be missed entirely. Studies using velocity-encoded cine-GRE (VEC) of the cross section of the shunt stream at the orifice allowed identification and assessment of ASD size that is not apparent in the magnitude image. This technique can yield ASD dimensions and shape with sufficient accuracy and can identify patients, who require surgical repair versus those who may be suitable for non-surgical ASD closure by catheterisation techniques [3]. Velocity-encoded cine-GRE is also an accurate and reproducible method for measuring Q_p/Q_s . Use of velocity-encoded GRE to demonstrate unequal levels of pulmonary and systemic flows in a few patients with various forms of congenital heart disease has already been reported [4]. Studies have demonstrated that velocity-encoded GRE can quantify Q_p/Q_s in patients with a left to right shunt and that these results correlate closely with oximetric data obtained at cardiac catheterization [5].

Ventricular Septal Defect

Ventricular septum defects (VSD) can be diagnosed by either SE pulse-sequences using transverse or coronal planes or by

From the Department of Internal Medicine, Donauklinikum Tulln, Austria
Correspondence to: Prim. Univ.-Prof. Dr. med. Herbert Frank, Abteilung für Innere Medizin, Donauklinikum Tulln, Alter Ziegelweg 50, A-3430 Tulln;
E-Mail: interne@donauklinikum.at

GRE technique. Despite the reported accuracy with SE imaging, small ventricular septal defects will be missed and muscular defects not identified. GRE imaging, however, has resulted in improved detectability of VSD because the actual shunt flow is identified. The overall sensitivity of MRI in diagnosis of VSDs was calculated to be 100 % at the 95 % specificity levels [1]. Defects in the trabecular portion of the septum can be identified very easily by MRI. These defects penetrate the muscular septum, are surrounded entirely by muscle, and are not related to the aortic or atrioventricular valve. Conoventricular defects, characteristically with one border formed by the mitral, tricuspid, and aortic fibrous continuity, are often seen on transverse SE images. The morphology of this defect and its relationship to the septal leaflet of the tricuspid valve are particularly important because some of these defects are partially covered by the valvular structure, making the defect appear relatively small. Also important is the relationship of this defect to the aortic valve [6]. In these cases, selection of a small slice thickness of 5 mm is very important for accurate diagnosis. Supracristal defects are usually related to the pulmonary and aortic valves and are clearly demonstrated by contiguous transverse sections upward to the plane of the pulmonary valve.

Patent Ductus Arteriosus (Fig. 1)

An important application of MRI is in visualization of a patent Ductus arteriosus. Compared to other non-invasive imaging techniques, MRI allows detection and measurement of the extent of a patent Ductus arteriosus. The best demonstration is by transverse sections at the level of the great arteries and by coronal sections. The left anterior oblique plane in SE- and GRE-technique is very helpful in visualizing the ductus and verifying blood flow between aorta and pulmonary artery. Best results are achieved, if a slice thickness between 3 mm and 5 mm is selected. However, the accuracy of MRI for diagnosis of a patent Ductus arteriosus is still uncertain [6].

Anomalous Venous Connection

Although echocardiography is superior to MRI for detection of valvular abnormalities, MRI is better for showing anomalies of



Figure 1: Left anterior oblique plane in SE-technique of a patent ductus arteriosus (arrow)

pulmonary venous connection [7]. Visualization of pulmonary veins and diagnosis of an anomalous venous connection requires performing the MRI study with this intention. Partial anomalous pulmonary venous connection (PAPVC) is identified from the course of the pulmonary veins to their point of drainage and by demonstration of lack of communication to the left atrium on one side and the route of the anomalous connection on the other. The pulmonary veins may be connected to various sites, commonly classified as supracardiac, cardiac, infracardiac and mixed. Supracardiac connection is to the right superior vena cava (Fig. 2) or to the innominate vein. Cardiac connection may be to the coronary sinus or directly to the right atrium. Infracardiac connection is through a vertical vein to the inferior vena cava. Transverse SE-sections at the level of the left atrium and at the anomalous connection identify the anomaly. Sections of the lung at different levels and the inferior vena cava on transverse and coronal sections can also delineate anomalous drainage of the pulmonary veins.

Tetralogy of Fallot

Tetralogy of Fallot is a complex lesion with ventricular septal defect, aortic override of the defect, right ventricular outflow obstruction and right ventricular hypertrophy. A frequent associated anomaly is a right-sided aortic arch. The association of tetralogy of Fallot and absence of pulmonary valve leads to enlarged pulmonary arteries, which may cause bronchial obstruction.

MR tomograms in transverse, sagittal and coronal plane demonstrate all characteristic lesions of tetralogy of Fallot. The dimensional difference between aorta and pulmonary artery is revealed on transverse images. Sequential transverse and sagittal images can be used to demonstrate pulmonary stenosis. Sagittal images are helpful in the assessment of right ventricular wall thickness [8]. Pulmonary and bronchial arteries can be distinguished on transverse planes at the level of the carina. The origin of bronchial arteries from the descending aorta can be visualized on transverse and coronal images. Cine MRI has been used to demonstrate the right ventricular outflow tract and to identify pulmonary regurgitation [9] which particularly occurs when a transannular patch is used for relief of the outflow tract obstruction of the right ventricle. In case of residual pulmonary regurgitation, right ventricular overload may predispose to development of ventricular arrhythmia, a risk factor for sudden death. Several studies suggest that postoperative pulmonary regurgitation may be partly responsible for abnormal right ventricular haemodynamics or limited exercise capacity in otherwise asymptomatic patients with tetralogy of Fallot [10, 11]. Attempts have been made to estimate severity of pulmonary regurgitation using Doppler echocardiography, contrast ventriculography or videodensitometry. VEC-MR provides measurement of volumetric flow and is an accurate and non-invasive method for volumetric quantitation of pulmonary regurgitation in patients after surgical repair of tetralogy of Fallot [12]. In addition, the ability of MRI to measure right ventricular volumes tomographically allows a more comprehensive study of pulmonary regurgitation in postoperative tetralogy of Fallot.

MRI provides good visualization of vessel morphology and mediastinal structures, and is superior to echocardiography in

detection of additional vessel abnormalities, such as left brachiocephalic truncus and dextropositioned aorta. In tetralogy of Fallot associated with absence of the pulmonary valve, MRI makes imaging of the bronchial system possible and enables diagnosis of airway obstruction. Neither ultrasonic nor radiographic examinations allow accurate assessment of bronchus anatomy or malstructure. This additional information in tetralogy of Fallot, and in complex congenital heart disease in general, is necessary for preoperative assessment and planning of surgery [13].

Complete Transposition

In D-transposition of great arteries the aorta arises anteriorly from the right ventricle, whereas the pulmonary artery arises posteriorly from the left ventricle. In L-transposition, the morphologic left ventricle lies to the right, the morphologic right ventricle to the left. In this congenitally-corrected aortopulmonary transposition, there is an atrioventricular and ventriculoarterial discordance.

Transverse and coronal scans of the heart base reveal the origin of pulmonary artery and aorta. The anatomic right ventricle is recognized by the moderator band. In complete D-transposition, sequential transverse images show the anatomic right ventricle with an originating right-sided aorta. Right atrium and right ventricle are normally connected. In transverse MR tomograms, the aorta is anteriorly positioned and to the right of the pulmonary artery. In congenitally-corrected L-transposition, the aorta is visualized anterior and to the left of the pulmonary artery. Additional planes are needed to distinguish aorta and pulmonary artery unequivocally. The pulmonary artery may be recognized by following transverse images cranially to the pulmonary arterial bifurcation, whereas the ascending aorta is characterized by the aortic arch and brachiocephalic vessels.

The advantage of MRI in congenital heart disease is that additional malformations can be visualized due to the greater field of view. Several other congenital heart anomalies are associated with L-transposition, and can so be detected by MRI. The most frequent additional malformations are ventricular septal defect, valvular and subvalvular pulmonic stenosis, and Ebstein's anomaly of the left-sided atrioventricular valve.

Truncus Arteriosus

Truncus arteriosus is a common vessel that overrides both ventricles and the large ventricular septal defect. Coronary arteries, systemic and pulmonary vessels arise from this common vessel. The branching pattern into pulmonary and aortic circulations allows classification of the different forms of truncus arteriosus [14]. In type I truncus, there is a common pulmonary artery arising from the truncus, whereas the branch pulmonary arteries arise separately in type II truncus. In type III truncus, one of the branch pulmonary arteries is absent and one pulmonary artery is fed from a persistent patent Ductus arteriosus. Type IV truncus represents coincidence of a type I truncus with aortic arch interruption, where the ascending aorta is small and the descending aorta is perfused through a widely patent Ductus arteriosus. Transverse SE-sequences are recommended for visualization and classification of the different forms of truncus arteriosus. The site of origin of the pulmonary arteries can be discerned using thin slices (5 mm) on transverse or coronal tomograms. MRI can reliably classify truncus arteriosus by assessing pulmonary artery anatomy. The size of pulmonary artery and of its branches can be measured on transverse, coronal and sagittal planes. For assessment of pulmonary arteries a slice thickness of 3–5 mm is recommended.

■ Cardiac Masses

Magnetic resonance imaging (MRI) provides a non-invasive and three-dimensional assessment of masses involving the cardiac chambers, the pericardium, and the extracardiac structures. MRI has become an established method to yield complementary diagnostic information and to guide cardiac surgeons in the design of an appropriate therapeutic strategy. Furthermore, MRI allows to some extent characterization of tumour tissue. The goal of MRI for assessing cardiac and paracardiac masses includes (1) to confirm or to exclude a mass suspected by X-ray or echocardiography, (2) to assess the location, mobility and its relationship to surrounding tissues, (3) to image the degree of vascularization, (4) to distinguish solid from fluid lesions, and (5) to determine tissue characteristics and the specific nature of a mass.

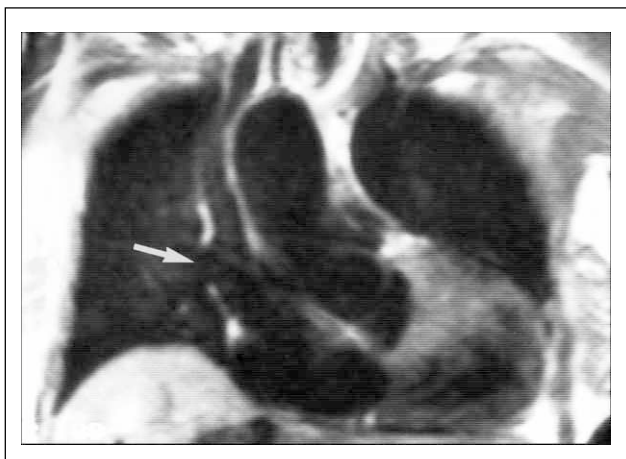


Figure 2: Coronal T1-weighted sections delineates the anomalous drainage of the pulmonary veins into the superior vena cava



Figure 3: Axial GRE-sequence demonstrating a myxoma (5 cm in diameter) in the left atrium. Typically, the myxoma shows low signal intensity at GRE-sequences, areas of increased signal intensity are consistent with haemorrhage

■ Benign Tumours of the Heart

Primary tumours of the heart are very rare, with an incidence between 0.0017 and 0.19 percent in unselected patients at autopsy. Three quarters of the tumours are benign and nearly half of them are myxomas and about 10 % are lipomas [15–21]. Rhabdomyomas, fibromas, haemangiomas, teratomas, and mesotheliomas are found less frequently. Granular cell tumours, neurofibromas and lymphangiomas are very rare [22].

Myxoma (Fig. 3)

Myxomas comprise 30 % to 50 % of all primary cardiac tumours and usually occur sporadically between the third and sixth decade of life [23]. In about 75 percent myxomas originate from the left atrium, and in 15 to 20 percent from the right atrium. They usually develop from the interatrial septum close to the fossa ovalis. Only a few myxomas are located in the ventricles. The histologic structure shows typically a myxoid matrix, large blood vessels at the base and often cysts and areas of haemorrhage and calcification [24]. They are generally polypoid, often pedunculated, round or oval with a smooth surface, often covered with thrombi and ranges in tumour size between 1 to 15 cm in diameter [15]. Clinical symptoms appear as a consequence of embolism or intracardiac obstruction and are determined by size, location and mobility of the myxoma [25, 26].

On MRI, myxomas are mainly diagnosed by the typically pedunculated, jelly-like and prolapsing appearance and certain SI characteristics [27]. Therefore, cine display should be obtained to show the mobility of the tumour [28]. Due to the endocardial origin, myxomas are characterized by an intermediate, but variable SI on SE-images, similar to that of myocardium. On gradient echo images, myxomas often have a low SI, which is caused by partial calcification. Therefore the tumour can always be distinguished from the higher SI of the surrounding slowly flowing blood [29, 30]. Intratumorous areas of subacute or chronic haemorrhage are typically characterized by high signal intensity on both short and long echo times [31]. Caused by vascularisation, myxomas show a moderately high contrast enhancement after i.v. administration of Gd-DTPA [16, 29].

Lipoma

Cardiac lipomas are the second most frequent benign tumour of the heart [22]. True lipomas are encapsulated, contain neoplastic fat cells and occur in young age [32, 33]. About 50 % arise subendocardially, 25 % subepicardially, and 25 % from the myocardium [34]. Subepicardial lipomas may become quite large and may alter cardiac function resulting in dyspnoea or fatigue [35], even an involvement of the coronary arteries is reported [36]. Endocardial lipomas commonly arise from the interatrial septum and are located in the right atrium. Arrhythmias due to myocardial infiltration have been reported [37]. Lipomatous hypertrophy of the atrial septum is histologically characterized by infiltration of lipomatous cells between atrial muscle fibers. Unlike true lipomas they are unencapsulated and contain lipoblasts as well as mature fat cells [38]. It has been classically described in older, overweight patients who have frequently atrial fibrillation [39].

On MRI, lipomas are characterized by bright SI on T1-weighted images and a slight decrease in SI on T2-weighted images similar to subcutaneous fat [17]. The administration of Gd-

DTPA is not needed because SI will remain unchanged. A decrease in SI using fat pre-saturation technique verifies the diagnosis. In lipomatous hypertrophy a bi-lobed atrial septum thickening with a signal intensity comparable to subcutaneous fat on T1- and T2-weighted images can be visualized. In contrast to the benign lipomatous hypertrophy of the interatrial septum the very rare observed liposarcoma shows usually infiltration, inhomogeneities and fast tumour growth [41].

Fibroma

Fibromas occur primarily in infants and children. They are congenital tumours frequently discovered in young adults [42]. Typically, fibromas are located intramyocardial within the ventricular septum. The left ventricle is more often involved than the right ventricle. Surgical excision is recommended even in asymptomatic patients [43], due to the potential risk of sudden death caused by arrhythmias.

On T1-weighted SE images, fibromas are isointense or slightly hyperintense compared to skeletal muscle. Due to the short T2-relaxation time of fibrous tissue, fibromas show a decrease in SI relative to the myocardium from T1- to T2-weighted SE images [44, 45].

A possible problem in diagnosing fibrous tissue might be the presence of fibromuscular elements within the right atrium. Small nodular soft-tissue structure isotense to myocardium and nodule or linear strands in the right atrium are commonly visible and may simulate a tumour [46]. These structures are representing variable degrees of remnants of the crista terminalis and the Chiari network in humans [47].

Rhabdomyoma

Rhabdomyomas are congenital tumours mainly diagnosed in newborn infants. Usually they arise from the ventricular myocardium at multiple locations. In about 50 % of patients tuberos sclerososis can be observed [48]. Rhabdomyoma have typically a solid and homogeneous appearance, which is hypointense to the myocardium on T1-weighted images and slightly hyperintense on T2-weighted images [49].

Cardiac Haemangioma

There are only few cases reported on arteriovenous haemangioma of the interventricular septum of the heart. The location of the tumour is predominantly the right or left ventricle, also septal involvement and multiple locations have been reported [50]. The distinction between a haemangioma and a vascular malformation may be difficult [51]. On MRI, haemangioma are characterized as a region of increased signal intensity on T1-weighted images compared to the myocardium due to slow flowing blood. After i.v. administration of Gd-DTPA the vascular nature of the tumour can be easily visualized [52].

Leiomyomatosis with Intracardiac Extension

The intravenous leiomyomatosis is a rare pathological entity and all tumours were observed in females, most of them were white and pre-menopausal [53]. The tumour arise either from an uterine myoma, or from the wall of the vessel [54]. It gen-

erally appears as a large mobile mass in the right atrium. Since the preoperative evaluation should include assessment of all cardiac chambers and the region of the inferior vena cava, MRI can be considered to be a primary diagnostic method [55]. Due to the myomatous tissue, SI characteristics are similar to that of muscle (Fig. 4).

■ Malignant Tumours of the Heart

Nearly 25 % of all cardiac tumours are malignant tumours. Metastatic formations are 20 to 40 times more common than primary malignant tumours and appear in 6 % of post-mortem autopsies in malignant diseases. The most common primary malignant cardiac tumours are various sarcomas and lymphomas [56, 57].

Due to the small number of studied cardiac malignancies, and the differences in tumour age, vascularisation and a widespread variability in water content, a reliable tissue differentiation of cardiac malignancies is still not possible [58, 59]. Distinct features of malignant tumours are the presence of necrosis, calcification, a high degree of vascularisation, infiltration of the adjacent tissues, inhomogeneous appearance and peritumorous oedema [60, 61].

Sarcoma

There exist various histologic types of sarcoma, such as angiosarcomata, leiomyosarcomata and liposarcomata [22, 57].

An *angiosarcoma* (Fig. 5) is the most frequent primary malignant cardiac tumour [22]. It is usually located within the right atrium and arises from the interatrial septum. In contrast, other types of sarcoma also occur in the left side of the heart, where they are often clinically mistaken for myxoma. Typically an angiosarcoma shows a polymorphical configuration with a central region of hyperintensity, consistent with necrosis, and moderate SI in peripheral regions in T1- and T2- weighted MR images [30]. Due to the high degree of vascularisation, signal enhancement is seen after i.v. administration of Gd-DTPA.

Primary *leiomyosarcomata* arise in 75 % from the inferior vena cava, but also have been reported with an origin of the superior vena cava [62]. This neoplasm demonstrates a signal



Figure 4: Axial T2-weighted pulse sequence of an echinococcus cyst located in the interventricular septum. Signal increase of the cyst typically found on the T2-weighted image

intensity on T1-weighted SE images slightly higher than liver parenchyma, but not as bright as the adjacent mediastinal fat. The advantage of MR imaging is the ability to assess the tumour extension both in the vena cava superior and into the heart chambers [63].

Liposarcomata often have a pericardial origin and MRI is able to detect this pericardial mass with heterogeneous high SI and epicardial infiltration. After administration of Gd-DTPA, liposarcomata may only show a slight signal enhancement [64].

Lymphoma

In T1- and T2-weighted SE images lymphomas appear isointense or hypotense to cardiac muscle. After administration of Gd-DTPA, lymphomata appear heterogeneous with less enhancing central regions consisting necrosis [59]. Post mortem studies have shown a cardiac involvement in up to 25 % of lymphoma, however, *in vivo* diagnosis is still rare [60].

Metastatic Tumours

There are three ways of metastatic tumours into the cardiac tissue: 1) direct mediastinal infiltration of heart tissue in case of lung cancer, breast cancer or mediastinal lymphomas, 2) metastatic formation by systemic tumours such as malignant melanoma, lymphoma, leukaemia and sarcoma, 3) transvenous spreading from the vena cava inferior in case of renal or hepatic tumours and transvenous spreading from the vena cava superior in case of lung cancer [22, 35].

■ Intracardiac Thrombus Formation

Intracardiac thrombus is often located in the left atrium in case of chronic atrial fibrillation and dilatation or in the left ventricle in case of wall motion abnormalities after myocardial infarction [65]. The diagnosis of cardiac thrombus is clinically



Figure 5: Axial SE-sequence (T1) of an angiosarcoma after administration of Gd-DTPA in a 85-year old woman. Compared to the myocardium, the tumour shows inhomogeneous, hyperintense signal intensity with infiltration of the right ventricular myocardium and the right atrial wall. Note the pericardial effusion.

important to identify patients at risk for systemic or pulmonary embolisation [66, 67]. However, in most cases the diagnosis of cardiac thrombi is coincidental and patients are asymptomatic. Despite the fact that 2D echocardiography is the method of choice for diagnosis, false positive rates as high as 28 % [68] in detection of left ventricular thrombi and 59 % in left atrial thrombi [69] have been reported.

On MRI images, fresh thrombi on T1-weighted SE images have often a higher SI than myocardium and the contrast is further accentuated on T2-weighted SE images consistent with a high amount of haemoglobin [65]. However, depending on the age of the thrombus alterations in SI are possible. After one or two weeks paramagnetic compounds of the organizing thrombus like desoxyhaemoglobin and methaemoglobin cause T1- and T2-shortening, which may result in increased SI in T1- and decreased SI in T2-weighted images [70]. Chronic organized thrombi are of low SI in consequence of loss of water and protons. A problem concerning differentiation between thrombus and slow flowing blood occurs especially in laminated or immobile thrombi on SE images [71]. Compared to thrombus formation, slow flowing blood shows an increasing SI on T2-weighted images [44, 72]. On GRE images a thrombus always has the lowest SI than all other cardiac structures, while blood appears brightest [70]. If thrombi contain calcifications, they appear more heterogeneous [31]. To differentiate thrombus from tumour, i.v. administration of contrast agents may be helpful. Thrombi usually do not show signal enhancement after intravenous administration of Gd-DTPA, unless they are already organized [9]. Compared to other diagnostic procedures MRI and CT offer a similar sensitivity of about 90% with a slightly better specificity as compared to two-dimensional echocardiography [71].

Pericardial Lesions

Magnetic resonance evaluation of pericardial neoplasm in most cases involves identification of abnormal anatomic structures and boundaries rather than characterization of relative tissue intensities. A few exceptions to this are included in the differential diagnosis of mediastinal masses, such as fibroma, lipoma and pericardial cysts. The value of MRI for evaluation of potential neoplasm lies largely in treatment planning and particularly preoperative assessment. The loss of normal anatomic boundaries is an important sign of neoplasm. Neoplastic involvement of the pericardium results in focal and diffuse obliteration of the normal pericardial signal. In the case of malignancy adjacent to cardiac structures, visualization of the pericardial line is an indication that pericardial invasion has not occurred.

Conclusion

Cardiovascular MRI techniques have contributed significantly to the ability to detect cardiac and paracardiac masses and play an important role in the diagnostic evaluation of cardiac and paracardiac masses complementary to echocardiography. Magnetic resonance imaging due to its larger field of view, adds diagnostic information by assessing extracardiac components of a mass, such as mediastinal involvement and extension into large pulmonary vessels. MRI allows to ex-

clude hiatal hernia, a tortuous descending aorta or a bronchogenic cyst, which can mimic cardiac tumours. MR-findings are helpful in defining paracardiac masses and in guiding therapeutic strategies. Tissue characterization by MRI is limited to the diagnosis of myxomas, fibromas, thrombi, pericardial cysts and fatty tissue. The signal features of malignant tumours are ambivalent and do not permit a tissue diagnosis. However, the inhomogeneous appearance of signal enhancement after the administration of Gadolinium-DTPA, the infiltrative components of a tumour and a hemorrhagic pericardial effusion makes the diagnosis of tumour malignancy possible.

References

1. Kersting-Sommerhoff B, Diethelm L, Teitel D, et al. Magnetic resonance imaging of congenital heart disease: sensitivity and specificity using receiver operating characteristic curve analysis. *Am Heart J* 1989; 118: 155-61.
2. Theissen P, Sechtem U, Mennicken U, et al. Noninvasive diagnosis of atrial septal defects and anomalous pulmonary venous return by magnetic resonance imaging. *Nuklear Medizin* 1989; 28: 172-80.
3. Holmvang G, Palacios I, Vlahakes G, et al. Imaging and sizing of atrial septal defects by magnetic resonance. *Circulation* 1995; 92: 3473-80.
4. Rees S, Firmin D, Mohiaddin R, et al. Application of flow measurements by magnetic resonance velocity mapping to congenital heart disease. *AJC* 1989; 64: 953-6.
5. Brenner L, Caputo G, Mostbeck G, et al. Quantification of left to right atrial shunts with velocity-encoded cine nuclear magnetic resonance imaging. *JACC* 1992; 20: 1246-50.
6. Soto B, Cranney G, Blackwell G. Congenital Heart disease in adult. In: Blackwell G, Cranney G, Pohost G (ed). *MRI: Cardiovascular System*. Gower Medical, New York, 1992.
7. Fellows K, Weinberg P, Baffa J, et al. Evaluation of congenital heart disease with MR Imaging: Current and coming attractions. *AJR* 1992; 159: 925-31.
8. Higgins C, Caputo G. Role of MR imaging in acquired and congenital cardiovascular disease. *AJR* 1993; 161: 13-22.
9. Chung K, Simpson I, Newman R, et al. Cine magnetic resonance imaging for evaluation of congenital heart disease: role in pediatric cardiology compared with echocardiography and angiography. *J Pediatr* 1988; 113: 1028-35.
10. Bove E, Byrum C, Thomas F, et al. The influence of pulmonary insufficiency on ventricular function following repair of tetralogy of Fallot. *J Thorac Cardiovasc Surg* 1983; 85: 691-6.
11. Homeffer P, Zahka K, Rowe S, et al. Long-term results of total repair of tetralogy of Fallot in childhood. *Ann Thorac Surg* 1990; 50: 179-85.
12. Rebergen S, Chin J, Ottenkamp J, et al. Pulmonary regurgitation in the late postoperative follow-up of tetralogy of Fallot: Volumetric quantitation by nuclear magnetic resonance velocity mapping. *Circulation* 1993; 88: 2257-66.
13. Frank H, Salzer U, Popow C, et al. Magnetic resonance imaging of absent pulmonary valve syndrome. *Pediatr Cardiol* 1996; 17: 35-9.
14. Calder L, Van Praagh R, Van Praagh S, et al. Truncus arteriosus communis. Clinical, angiographic and pathologic findings in 100 patients. *AJH* 1976; 92: 23-38.
15. Hall RJ, Cooley DA, Mac Allister HR Jr, Frazier OH. Neoplastic heart disease. In: Hurst JW (ed). *The heart, arteries and veins*. 7th ed. McGraw-Hill, New York, 1990: 1382-403.
16. Weinmann HJ, Lanaida M, Mutzel W. Pharmacokinetics of Gd-DTPA/dimeglumine after IV injection. *Physiol Chem Phys Med NMR* 1984; 16: 167-72.
17. Edelstein WA, Bottomley PA, Hart HR, Smith LS. Signal, noise, and contrast in nuclear magnetic resonance imaging. *J Comput Assist Tomogr* 1983; 7: 391-401.
18. Benjamin HG. Primary fibromyxoma of the heart. *Arch Pathol* 1939; 27: 950.
19. Heath D. Pathology of cardiac tumours. *Am J Cardiol* 1968; 21: 315-27.
20. Straus R, Merliiss R. Primary tumour of the heart. *Arch Pathol* 1945; 39: 74-8.
21. Wold LE, Lie JT. Cardiac myxomas: a clinicopathologic profile. *Am J Pathol* 1980; 101: 219-40.
22. Mc Allister HA Jr, Fenoglio JJ Jr. Tumours of the cardiovascular system. *Atlas of tumour pathology*. 2nd series. Fascicle 15. Armed Forces Institute of Pathology, Washington, D.C., 1978; 1-20.
23. Reynen K. Cardiac myxomas: review article. *N Engl J Med* 1995; 333: 1610-7.
24. Pritchard RW. Tumours of the heart. Review of the subject and report of one hundred and fifty cases. *Arch Pathol* 1951; 51: 98-128.
25. St John Sutton MG, Mercier L-A, Giuliani ER, Lie JT. Atrial myxomas. A review of clinical experience in 40 cases. *Mayo Clin Proc* 1980; 55: 371-6.
26. Peters MN, Hall RJ, Cooley DA, Leachmann RD, Garcia E. The clinical syndrome of atrial myxoma. *JAMA* 1974; 230: 695-701.
27. Lund JT, Ehman RL, Julsrud PR, Sinak LJ, Tajik AJ. Cardiac masses. Assessment by MRI. *Am J Radiol* 1989; 152: 469-73.
28. Go RT, O'Donnell JK, Underwood DA, Feiglin DH, Salcedo EE, Pantoja M, MacIntyre WJ, Meaney TF. Comparison of gated cardiac MRI and 2D Echo of intracardiac neoplasms. *Am J Radiol* 1985; 145: 21-5.
29. Semelka RC, Shoenuit JP, Wilson ME, Pellech AE, Patton JN. Cardiac masses. Signal intensity features on spin-echo, gradient-echo, gadolinium-enhanced-spin-echo, and TurboFLASH images. *J Magn Reson Imaging* 1992; 2: 415-20.
30. Gomes AS, Lois JF, Child JS, Brown K, Batra P. Cardiac tumours and thrombus. Evaluation with MR imaging. *Am J Radiol* 1987; 149: 895-9.
31. Roos A, Weijers E, Duinen S, Wall EE. Calcified right atrial myxoma demonstrated by MRI. *Chest* 1989; 95: 478-9.
32. Reyes CV, Jablakov VR. Lipomatous hypertrophy of the cardiac interatrial septum. A report of 38 cases and review of the literature. *Am J Clin Pathol* 1979; 5: 785-8.
33. Crocker DW. Lipomatous infiltrates of the heart. *Arch Pathol Lab Med* 1978; 102: 69-72.
34. Fine G. Neoplasms of the pericardium and heart. In: Gould SE (ed). *Pathology of the heart and blood vessels*. 3rd ed. Charles C. Thomas, Springfield, 1968; 865.

35. Moulton AL, Jaretzki AIII, Bowman OF, Silverstein EF, Bregman D. Massive lipoma of the heart. *NY State J Med* 1976; 76: 1820-5.
36. Hananouchi GI, Goff WB. Cardiac lipoma. Six-year follow-up with MRI characteristics, and a review of the literature. *Magn Reson Imaging* 1990; 8: 825-8.
37. Conces DJ, Vix VA, Tarver RD. Diagnosis of a myocardial lipoma by using CT. *AJR* 1989; 153: 725-6.
38. Hutter Am Jr, Page DL. Atrial arrhythmias and lipomatous hypertrophy of the cardiac interatrial septum. *Am Heart J* 1971; 82: 16-21.
39. Kluge WF. Lipomatous hypertrophy of the interatrial septum. *Northwest Med* 1969; 68: 25-30.
40. Levine RA, Weyman AE, Dinsmore RE, Southern J, Rosen BR, Guyer DE, Brady TJ, Okada RD. Noninvasive tissue characterization. Diagnosis of lipomatous hypertrophy of the atrial septum by Nuclear MRI. *J Am Coll Card* 1986; 7: 688-92.
41. Applegate PM, Tajik AJ, Ehman RL, Julsrud PR, Miller FA. Two-dimensional echocardiographic and MRI observations in massive lipomatous hypertrophy of the atrial septum. *Am J Card* 1987; 59: 489-91.
42. Burke AP, Rosado CM, Templeton PA, Virmani R. Cardiac fibroma. Clinicopathologic correlates and surgical treatment. *J Thorac Cardiovasc Surg* 1994; 108: 862-70.
43. Oliva PB, Breckinridge JC, Johnson ML, Brantigan CO, O'Meara OP. Left ventricular outflow obstruction produced by a pedunculated fibroma in a newborn. Clinical, angiographic, echocardiographic and surgical observations. *Chest* 1978; 74: 590-3.
44. Winkler M, Higgins CB. Suspected intracardiac masses. Evaluation with MR Imaging. *Radiology* 1987; 165: 117-22.
45. Gamsu G, Stark DD, Webb WR, Moore EH, Sheldon PE. MRI of benign mediastinal masses. *Radiology* 1984; 151: 709-13.
46. Meier RA, Hartnell GG. MRI of right atrial pseudomass. Is it really a diagnostic problem? *J Comput Assist Tomogr* 1994; 18: 398-401.
47. Edwards JE. Congenital malformations of the heart and great vessels. In: Gould SE (ed). *Pathology of the heart*. Bannerstone House, Springfield, IL, 1960; 61-3.
48. Abushaban L, Denham B, Duff D. 10 year review of cardiac tumours in childhood. *Br Heart J* 1993; 70: 166-9.
49. Hoffmann U, Globits S, Frank H. Cardiac and paracardiac masses. Current opinion an diagnostic evaluation by magnetic resonance imaging. *Eur Heart J* 1998; 19: 166-9.
50. Brizard C, Latremouille C, Jebara VA, Acar C, Fabiani JN, Deloche A, Carpentier AF. Cardiac hemangiomas. *Ann Thorac Surg* 1993; 56: 390-4.
51. Newell II JD, Eckel C, Davis M, Tadros NB. MR appearance of an arteriovenous hemangioma of the interventricular septum. *Cardiovasc Intervent Radiol* 1988; 11: 319-21.
52. Soberman MS, Plauth WH, Winn KJ, et al. Hemangioma of the right ventricle causing outflow obstruction. *J Thorac Cardiovasc Surg* 1988; 96: 307-9.
53. Spellacy WN, Maire WJ, Buhi WC. Plasma growth hormone and estradiol. Levels in woman with uterine myomas. *Obstet Gynecol* 1972; 40: 829-34.
54. Bassish MS. Mesenchymal tumours of the uterus. *Clin Obstet Gynecol* 1974; 17: 51-88.
55. Rosenberg JM, Marvasti MA, Obeid A, Johnson LW, Bonaventura M. Intravenous leiomyomatosis. A rare cause of right sided cardiac obstruction. *Eur J Cardio Thorac Surg* 1988; 2: 58-60.
56. Roberts WC, Glancy DL, DeVita VT. Heart in malignant lymphoma. A study of 196 autopsy cases. *Am J Cardiol* 1968; 22: 85-107.
57. Silverman J, Olwin JS, Graettinger JS. Cardiac myxomas with systemic embolization. Review of the literature and report of a case. *Circulation* 1962; 26: 99-103.
58. Zeitler n. MRI of aneurysms and thrombi. *Cardiovasc Intervent Radiol* 1986; 8: 321-8.
59. Dorsay TA, Ho VB, Rovira MJ, Armstrong MA, Brisette MD. Primary cardiac lymphoma. CT and MR findings. *J Comp Assist Tomogr* 1993; 17: 978-81.
60. Hendrick RE, Raff U. Image contrast and noise. In Stark DD, Bradley WB (ed). *MRI*. Mosby-Year Book, St. Louis, 1992; 109-44.
61. Tazelaar HD, Locke TJ, McGregor CGA. Pathology of surgically excised primary cardiac tumours. *Mayo Clin Proc* 1992; 67: 957-65.
62. Lupetin AR, Dash N, Beckman I. Leiomyosarcoma of the superior vena cava. Diagnosis by cardiac gated MR. *Cardiovasc Intervent Radiol* 1986; 9: 103-5.
63. Somers K, Lotte F. Primary lymphosarcoma of the heart. Review of the literature and report of 3 cases. *Cancer* 1960; 3: 449-57.
64. Garrigue S, Robert F, Roudaut R, Bonnet J. Assessment of non-invasive imaging techniques in the diagnosis of heart liposarcoma. *Eur Heart J* 1995; 16: 139-41.
65. Doms GC, Higgins CB. MR imaging of cardiac thrombi. *J Comp Assist Tomogr* 1986; 10: 415-20.
66. Visser CA, Kan G, Meltzer RS, Dunning AJ, Roelandt J, van Corler M, de Koning H. Embolic potential of left ventricular thrombus after myocardial infarction. A two-dimensional echocardiographic study of 119 patients. *JACC* 1985; 5: 1276-80.
67. Hamby RI, Wisoff BG, Davison ET, et al. Coronary artery disease and left ventricular mural thrombi. Clinical, hemodynamic, and angiocardiographic aspects. *Chest* 1974; 66: 488-94.
68. Barakos JA, Brown JJ, Higgins CB. MR imaging of secondary cardiac and paracardiac lesions. *AJR* 1989; 153: 47-50.
69. Feigenbaum H. Coronary artery disease. In: Feigenbaum H (ed). *Echocardiography*. 4th ed. Lea and Febiger, Philadelphia, 1986; 489-94.
70. Jungehülsing M, Sechtem U, Theissen P, Hilger HH, Schicha H. Left ventricular thrombi. Evaluation with spin-echo and gradient-echo MR imaging. *Radiology* 1992; 182: 225-9.
71. Sechtem U, Theissen P, Heindel W, Hungerberg K, Deutsch HJ, Welslau R, Curtius JM, Huegel W, Höpp HW, Schicha H. Diagnosis of left ventricular thrombi by MRI and comparison with angiocardiography, computed tomography and echocardiography. *Am J Cardiol* 1989; 64: 1195-9.

ANTWORTFAX

JOURNAL FÜR KARDIOLOGIE

Hiermit bestelle ich

ein Jahresabonnement
(mindestens 6 Ausgaben) zum
Preis von € 60,- (Stand 1.1.2010)
(im Ausland zzgl. Versandkosten)

Name

Anschrift

Datum, Unterschrift

Einsenden oder per Fax an:

Krause & Pachernegg GmbH, Verlag für Medizin und Wirtschaft,
Postfach 21, A-3003 Gablitz, **FAX: +43 (0) 2231 / 612 58-10**

Bücher & CDs
Homepage: www.kup.at/buch_cd.htm
